PCCP

Accepted Manuscript

ROYAL SOCIETY OF CHEMISTRY

www.rsc.org/pccp

Physical Chemistry Chemical Physics
CREATED USING THE RSC LaTeX PCCP ARTICLE TEMPLATE – SEE www.rsc.org/electronicfiles FOR DETAILS
ARTICLE TYPE www. rsc.org/xxxxxx | XXXXXXXX

Nb and Ta Layer Doping Effects on the Interfacial Energetics and Electronic Properties of $LaAlO_3/SrTiO_3$ Heterostructure: First-Principles Analysis

Safdar Nazir[a], Maziar Behtash[a], Jianli Cheng[a], Jian Luo[a], and Kesong Yang*[a]

Received Xth XXXXXXXXXX 20XX, Accepted Xth XXXXXXXXX 20XX
First published on the web Xth XXXXXXXXXX 200X
DOI: 10.1039/b000000x

The two-dimensional electron gas (2DEG) formed at *n*-type $(LaO)^{+1}/(TiO_2)^0$ interface in polar/nonpolar $LaAlO_3/SrTiO_3$ (LAO/STO) heterostructure (HS) has emerged as a prominent research area because of its great potential for nanoelectronic applications. For its practical implementation in devices, desired physical properties such as high charge carrier density and mobility are vital. In this respect, 4*d* and 5*d* transition metal atom doping near the interfacial region is expected to tailor electronic properties of the LAO/STO HS system effectively. Herein, we studied Nb and Ta-doping effects on the energetics, electronic structure, interfacial charge carrier density and magnetic moment, and the charge confinements of the 2DEG at *n*-type $(LaO)^{+1}/(TiO_2)^0$ interface in LAO/STO HS using first-principles density functional theory calculations. We found that the substitutional doping of Nb (Ta) at Ti [Nb(Ta)@Ti] and Al [Nb(Ta)@Al] sites is energetically more favorable than that at La [Nb(Ta)@La] and Sr [Nb(Ta)@Sr] sites, and at appropriate thermodynamic conditions, the changes of the interfacial energy of HS systems upon Nb(Ta)@Ti and Nb(Ta)@Al doping are negative, implying that the formation of these structures is energetically favored. Our calculations also showed that Nb(Ta)@Ti and Nb(Ta)@Al doping significantly improve the interfacial charge carrier density with respect to that of the undoped system, which is because Nb (Ta) dopant introduces excess free electrons into the system, and these free electrons reside mainly on the Nb (Ta) ions and interfacial Ti ions. Hence, along with the Ti 3*d* orbitals, the Nb 4*d* and Ta 5*d* orbitals also contribute to the interfacial metallic states; accordingly, the magnetic moments on the interfacial Ti ions increase significantly. As expected, the Nb@Al and Ta@Al doped LAO/STO HS systems show higher interfacial charge carrier density than the undoped and other doped systems. In contrast, Nb@Ti and Ta@Ti doped systems may show higher charge carrier mobility because of the lower electron effective mass.

1 INTRODUCTION

In recent years, perovskite oxide heterostructures (HS) have been paid much attention due to the emergence of unexpected physical properties at their interfaces, which were absent in their individual parent compounds. For example, a considerable high charge carrier density ($\sim 10^{13}$ cm^{-2}) and highly-mobile ($\sim 10^4$ cm^2 V^{-1} s^{-1}) two-dimensional electron gas (2DEG) is observed at the *n*-type $(LaO)^{+1}/(TiO_2)^0$ interface between two insulating non-magnetic perovskite oxides, polar $LaAlO_3$ (LAO) and non-polar $SrTiO_3$ (STO).[1] The LAO/STO HS system also exhibits other material properties such as interfacial ferromagnetism and superconductivity,[2–6], colossal magnetoresistance[7,8] and electric-field controlled insulator-to-metal transition.[9,10] One of the widely accepted physical mechanisms behind the formation of metallic interfacial states in the STO-based HS systems is the *"polar catastrophe"* theory, in which charge transfers from the polar $(LaO)^{+1}$ layer of LAO to the non-polar $(TiO_2)^0$ layers of the STO substrate.[11] In addition, surface/interface defects such as oxygen vacancies[12–15] and cation-intermixing[16,17] were also proposed to be able to produce 2DEG.

Despite the diversified mechanisms on the formation of the 2DEG, recent concerted research efforts have been made to further tailor the electronic properties of 2DEG in the LAO/STO HS.[18–21] For example, applying an external electric field was found to be capable of tuning both carrier concentration and the required critical thickness of LAO to form a 2DEG at the interface.[10,22–25] Along with this, strain also shows prominent effects on the interfacial charge carrier density, electron confinement effects, and the LAO critical thickness for forming the 2DEG.[18,19,21,26,27] Another effective way to tune the electron transport properties of 2DEG in the LAO/STO HS is through transition-metal and rare-earth metal doping, which can significantly tune the electron transport properties.[28–32] For example, it has been experimentally and theoretically observed by Choi *et al.*[30] that fractional δ-doping of La at Sr site in STO/STO ($La_xSr_{1-x}TiO_3$/STO) HS system near the interfacial region could produce a high-mobility 2DEG. This is because one La^{3+} ion at a Sr^{2+} site

releases one an extra electron into the system, and the additional electron occupies the Ti 3*d* orbitals, leading to the formation of 2DEG. Blamire *et al.*[33] also found that inserting one unit cell of $ATiO_3$ (A = Ca, Sr, Sn, and Ba) at the interface between LAO and STO could significantly modulate the sheet carrier density of 2DEG. Their experimental measurements show that the Sn doping at La sites in the LAO/STO HS has the maximum carrier density. This conclusion is consistent with the recent first-principles electronic structure calculations that reveals the Sn doping near the interfacial region can significantly enhance the charge carrier density of 2DEG in LAO/STO HS system.[34] The main reason is that the Sn^{4+} doping at Al^{3+} sites introduces one additional electron into the HS system, which leads to the higher charge carrier density and even large magnetic moments on Ti ions. Hwang *et al.*[20] also found that inserting $LaTiO_3$(LTO) layers between LAO and STO can improve the charge carrier density in the LAO/STO HS, which is in agreement with first-principles calculations.[35] Very recently, Chen *et al.* found that a layer doping using $La_{1-x}Sr_xMnO_3$ (x=0, 1/8, and 1/3) at the interface (corresponds to the Mn doping at Al sites) between the disordered $LaAlO_3$ and crystalline $SrTiO_3$ could enhance the electron mobility by more than two orders of magnitude.[36] This experimental finding is very surprising, because the electron doping often plays a bigger role in improving the electron carrier density than in improving the electron mobility. Nevertheless, one possible underlying reason for the high electron mobility is that the Mn doping introduces Mn 3*d*-orbital related conducting states, which has a lower effective mass that Ti 3*d* orbitals related ones.[37] In spite of this intriguing experimental finding, one may speculate accordingly that the layer doping using 4*d* or 5*d*-based elements would be more effective in enhancing the electron transport property of the 2DEG in LAO/STO system since these less localized nature of 4*d*- and 5*d* orbitals will result in a smaller electron effective mass and thus potentially lead to a higher mobility. Consequently, it turns out that Nb and Ta doping at either Ti sites[38] in the STO substrate or Al sites in the LAO film would be a promising way to enhance the electron transport property of the LAO/STO HS system based on the two following considerations: i) Nb^{5+} (Ta^{5+}) doping at either Ti^{4+} sites or Al^{3+} doping would increase the interfacial charge carrier density; ii) Nb 4*d*- and Ta 5*d*-related conducting states may have high electron mobility. Hence, from the above viewpoints, it is necessary to study the Nb (Ta) doping influence on the materials properties of the LAO/STO HS system.

In this paper, thermodynamic stability, electronic, and magnetic properties of n-type $(LaO)^{+1}/(TiO_2)^0$ interfaces in LAO/STO HS systems were studied with respect to Nb(Ta)-doping at the Ti (Nb@Ti)/(Ta@Ti) and Al (Nb@Al)/(Ta@Al) sites near the interfacial region using first-principles electronic structure calculations. Our results indicate that Ta-doping at the Ti site (Ta@Ti) is more energetically favourable compared to the undoped and other doped LAO/STO HS systems. We predict that partial occupation of DOS effectively increases near the Fermi energy for Nb(Ta)@Ti doped LAO/STO HS systems, resulting in higher electron carrier density at the TiO_2 terminated $(LaO)^{+1}/(TiO_2)^0$ n-type interfaces. Furthermore, our calculations demonstrate that the mobile charges of 2DEG is confined within two TiO_2 atomic layers of the STO substrate for Nb@Al and Ta@Al doped LAO/STO HS systems, which improves the quantum confinement effects. Finally, the changes in calculated magnetic moments in undoped and Nb(Ta)-doped systems also show a similar pattern to that of exhibited by the partial occupation of DOS.

2 CALCULATION METHODS AND STRUCTURAL DETAILS

Our electronic structure calculations were performed in the framework of density functional theory using the Vienna *Ab-Initio* Simulation Package.[39] The spin-polarized generalized gradient approximation (GGA) parameterized by Perdew-Burke-Ernzerhof (PBE)[40] plus on-site Coulomb interaction approach (GGA+U) was applied for the exchange-correlation functional with U = 5.8 eV and 7.5 eV for Ti 3d and La 4f orbitals, respectively. The U value for Ti 3*d* states calculated from the constrained density functional theory[41] was proven accurate enough to provide a realistic description of the Ti 3*d* states.[18,38,42] The applied U value on La 4*f* electrons in this study is also suitable as discussed in prior work.[43,44] It is well-known that the on-site Coulomb repulsion energy U is much smaller for 4*d* and 5*d* electrons than for 3*d* electrons because the 4*d* and 5*d* orbitals are less localized.[45] The prior work shows that for the system with the co-existence of the Ti 3*d* and Nb 4*d* (Ta 5*d*) electrons, in which the electronic properties of the material system are mainly determined by Ti 3*d* orbitals, the U values for the 4*d*/5*d* orbitals can be neglected.[38]Hence, in this work, no U values are applied for Nb 4*d* and Ta 5*d* orbitals. The cut-off kinetic energy of 450 eV was used for the electronic wave function expansion. A $10 \times 10 \times 1$ k-space grid with 21 points in the irreducible wedge of the Brillöuin zone was found to converge appropriately. All crystal structures were optimized by minimizing the atomic forces upto 0.02 eV/Å, and self-consistency was assumed for a total energy convergence of less than 10^{-5} eV. A Gaussian smearing of 0.05 eV was used for density of states (DOS) calculations.

The parent compounds LAO and STO crystallize in cubic structures with space group no. 221 ($Pm\bar{3}m$). The experimental lattice parameters and energy gaps of these compounds are 3.789 Å/3.905 Å and 5.6 eV/3.2 eV for LAO and STO, respectively.[1] The calculated band gaps within the GGA+U scheme were 3.12 and 2.29 eV for LAO and STO, respectively. These

Table 1 Calculated Ti−O, Nb−O, Ta−O bond length (Å) along the *c*-axis, La−O bond length (Å) along the *ac*-plane and O−Ti−O, O−Nb−O, and O−Ta−O bond angles in the *ab*-plane near the interfacial region for undoped and Nb(Ta)-doped LAO/STO HS systems.

Bond	Undoped	Nb@Ti	Ta@Ti	Nb@Al	Ta@Al
Ti−O	2.04	-	-	2.16	2.19
Nb−O	-	2.11	-	-	-
Ta−O	-	-	2.14	-	-
La−O	2.72	2.86	2.83	2.59	2.53
O−Ti−O	172.4^o	-	-	169.4^o	167.9^o
O−Nb−O	-	175.2^o	-	-	-
O−Ta−O	-	-	174.3^o	-	-

values are underestimated compared to the experimental values and can be correctly predicted using hybrid functional calculations.[46–49] However, the underestimation of the band gap has no influence on our conclusions regarding the interfacial metallic states because the Ti 3*d* electronic states forming the metallic states can be well reproduced from the GGA+*U* calculations.[18,38,42] Moreover, previously it was confirmed that both the GGA+*U*[26] and HSE06[50] methods produced similar electronic properties regarding 2DEG in LAO/STO HS system. This indicates that the GGA+*U* approach is acceptable in estimating the Ti 3*d*-orbitals related electronic states. A supercell approach is used to model the $(LAO)_{6.5}/(STO)_{11.5}$ HS, where the subscripts 6.5 and 11.5 denote the number of unit cells of LAO and STO, respectively. The supercell is a single unit cell wide in the *a*- and *b*-directions, and contains two periodic *n*-type $(TiO_2)^0/(LaO)^{+1}$ symmetric interfaces. The experimental lattice constant of STO, 3.905 Å, is fixed in the *ab*-plane to construct all the HS systems, which lead to a lattice mismatch of 2.97% between the LAO film and the STO substrate. The Nb (Ta)-doped LAO/STO HS are modeled by replacing Ti (Nb@Ti)/(Ta@Ti) and Al (Nb@Al)/(Ta@Al) cations with Nb (Ta) near the interfacial region. Given that two symmetric interfaces are present in the periodic model, two such doped layers were introduced. This amounts to an intra-layer doping concentration of 100%, corresponding to the layer-doping model.[20,34–36,51] In fact, recent experimental work shows that the layer doping can be experimentally feasible via atomic layer control, which can be one effective approach to tune electronic properties for new functionalists in the designed HS.[20,36,51]

3 RESULTS AND DISCUSSION

3.1 Structural Relaxation and Thermodynamic Stability

It was already known that there is a significant octahedral distortion near the interfacial region of the LAO/STO HS, which substantially influence the interface electronic states.[43,52–54] To properly investigate this distortion, it is necessary to relax the undoped and doped HS systems. We accomplished this by fixing the *ab*-plane lattice parameters to that of the STO substrate (3.905 Å), while relaxing the atomic positions along the *z*-direction until the atomic forces were below 0.02 eV/Å. This approach has been used successfully on undoped LAO/STO systems in the past, mirroring experimental electronic properties quite well.[18,26,27] The calculated Ti−O, Nb−O, Ta−O bond distances along the *c*-axis, La−O bond distances in the *ac*-plane, and O−Ti−O, O−Nb−O, and O−Ti−O bond angles in the *ab*-plane near the interfacial regions are listed in Table 1 for undoped and Nb(Ta)-doped LAO/STO HS systems. In the Nb@Ti, Ta@Ti, Nb@Al, and Ta@Al doped systems, interfacial Nb−O, Ta−O, and Ti−O bond distances increased by 0.07, 0.10, 0.12, and 0.15 Å, respectively, compared to Ti-O bond in the undoped system. In contrast, the interfacial O−Nb−O and O−Ta−O bond angles decreased by 2.8^o and 1.9^o for the Nb@Ti and Ta@Ti doped systems, respectively, compared to O−Ti−O bond angle in undoped LAO/STO system. Similarly, O−Ti−O bond angles decreased by 3.0^o and 4.5^o for Nb@Al and Ta@Al doped systems. This means that TiO_6 octahedra is more distorted near the interfacial region when Ta is doped at the Al site (Ta@Al) than that of all the other doped and undoped LAO/STO HS systems. On the other hand, interfacial La−O bond distance along the *ac*-plane in the Nb@Al and Ta@Al doped systems substantially decreases by 0.13 and 0.19 Å, respectively, with respect to that of the undoped system, suggesting that the interfacial La−O bond becomes stronger if Nb or Ta substitutes on Al sites. In contrast, substitution of Nb or Ta on Ti sites appears to weaken the La-O bonds as interfacial La−O bond length increases by 0.14 and 0.11 Å in the case of Nb@Ti and Ta@Ti doped HS systems, respectively.

Next we evaluated the change of interfacial energetics between the undoped and Nb(Ta)-doped LAO/STO systems under various thermodynamic conditions using the following formula:

$$\Delta\gamma = \gamma_{Nb@X} - \gamma_{undoped} \quad (1)$$

where $\Delta\gamma$ is the interfacial energy difference between the Nb-doped ($\gamma_{Nb@X}$) and undoped ($\gamma_{undoped}$) LAO/STO systems (at 0 K) and X is the host ions that Nb replaces (X = Sr, Ti, La, and Al). If $\Delta\gamma$ is less than zero, it means the doped LAO/STO system is energetically more favorable than the undoped sys-

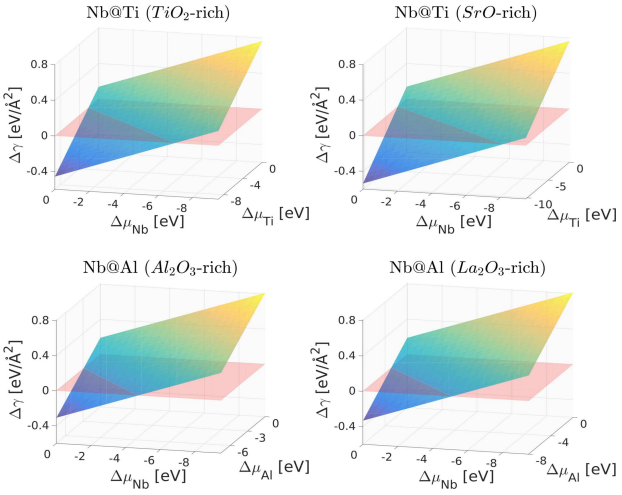

Fig. 1 Calculated change of the interfacial energy between Nb@X (X=Ti and Al) doped and undoped LAO/STO HS systems. The Nb@Ti doping (top row) was considered under TiO_2 and SrO-rich conditions, respectively. The Nb@Al doping (bottom row) was considered under Al_2O_3 and La_2O_3-rich conditions, respectively. The translucent red plane delineates $\Delta\gamma = 0$, the value below that means that doping is energetically favorable.

tem, that is, the doped system can be formed spontaneously. If $\Delta\gamma$ is larger than zero, it indicates that the doped LAO/STO system is energetically less favorable than the undoped system, that is, the doped system cannot be formed. As seen in the following equation, $\Delta\gamma$ depends on two variable chemical potentials (that of the dopant and host ions) which themselves depend on the thermodynamic condition.[55,56]

$$\Delta\gamma = (E_{HS}^{Nb@X} - E_{HS}^{undoped} + 2\mu_X - 2\mu_{Nb})/2A \quad (2)$$

$E_{HS}^{Nb@X}$ and $E_{HS}^{undoped}$ represent the total energies of the doped and undoped HS systems, respectively. It is noted here that, to , all energies used to determine the thermodynamic stability were derived from standard DFT calculations (without applying U parameters). μ_X (X = Sr, Ti, La, or Al) is the chemical potential of the host ion, while μ_{Nb} is the chemical potential of the Nb dopant. A is the interfacial area, while the factor of 2 preceding is due to the presence of two symmetrical interfaces in our model. Similarly, the factor of 2 preceding the chemical potentials indicates that two interfacial host ions are replaced by Nb.

Let us begin by considering the case of substitutional doping within the STO portion of the interface. As mentioned above, $\Delta\gamma$ is not fixed but depends on the chemical potentials of the dopant and host ions. In fact, the chemical potentials of the relevant elements are determined by the syntheses process in the experiment. In the STO portion, the chemical potentials of various elements are linked by its thermodynamic equilibrium condition:

$$\mu_{Sr} + \mu_{Ti} + 3\mu_O = E_{STO} \quad (3)$$

where μ_{Sr}, μ_{Ti}, and μ_O represent the chemical potentials of Sr, Ti, and O, while E_{STO} refers to the total energy of STO formula unit. It is important to note that for any particular dopant substitution, only the chemical potential of the displaced host ion is used in Equation 2. Determining this chemical potential at specific thermodynamic conditions, however, often requires consideration of the other linked chemical potentials as well. To avoid confusion regarding the chemical potential references, we have included the following definitions:

$$\Delta\mu_{Sr} = \mu_{Sr} - E_{Sr} \quad (4)$$

$$\Delta\mu_{Ti} = \mu_{Ti} - E_{Ti} \quad (5)$$

$$\Delta\mu_O = \mu_O - \frac{1}{2}E_{O_2} \quad (6)$$

E_{Sr} and E_{Ti} are the per-atom energy of the most stable low-temperature phases of elemental Sr and Ti, while E_{O_2} is the total energy of the isolated ground state O_2 molecule, both at 0 K. The formation enthalpy of STO is defined as:

$$\Delta H_f(STO) = E_{STO} - E_{Sr} - E_{Ti} - \frac{3}{2}E_{O_2} \quad (7)$$

which can be further rewritten as below using above definitions:

$$\Delta H_f(STO) = \Delta\mu_{Sr} + \Delta\mu_{Ti} + 3\Delta\mu_O \quad (8)$$

In fact, this equation must be satisfied to guarantee the stability of STO. Similar equations can be developed for LAO, which are relevant when considering substitutional doping within the LAO portion of the interface.

Returning to the interfacial energy difference (Equation 2), it is important to note that, experimentally, μ_X and μ_{Nb} strongly depend on the material growth conditions. Therefore, we considered a series of thermodynamic conditions and determined the relevant chemical potential ranges within those conditions. The specific conditions considered are: SrO-rich, TiO_2-rich, Al_2O_3-rich, and La_2O_3-rich. The former two conditions are relevant when considering doping on the STO side, while the latter two are used for doping at the LAO side. By using the definitions (4)-(6), the Equation 2 can be further rewritten as below:

$$\Delta\gamma = [E_{HS}^{Nb@X} - E_{HS}^{undoped} + 2(\Delta\mu_X - \Delta\mu_{Nb}) + 2(E_X - E_{Nb})]/2A \quad (9)$$

As an example let us consider Nb@Ti doping in the SrO-rich case. Under SrO-rich conditions, the following equation is always satisfied:

$$\Delta H_f(SrO) = \Delta\mu_{Sr} + \Delta\mu_O \quad (10)$$

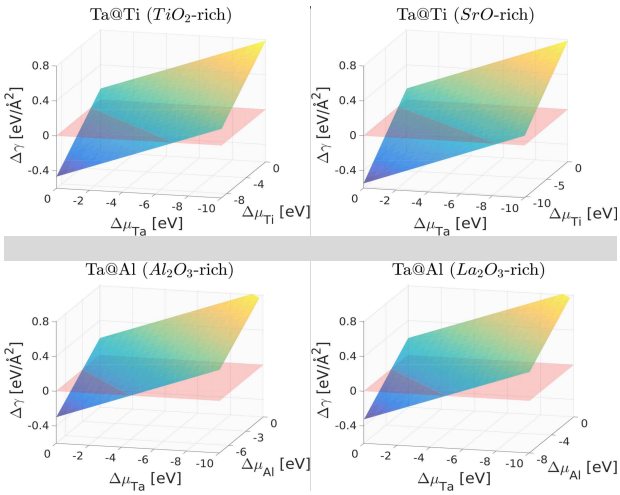

Fig. 2 Calculated change of the interfacial energy between Ta@X (X=Ti and Al) doped and undoped LAO/STO HS systems.

By splitting the SrO-rich condition into sub-conditions (O-rich, *i.e.,* $\Delta\mu_O$=0 and Sr-rich, *i.e.*, $\Delta\mu_{Sr}$=0) using thermodynamic laws, we were able to determine that the theoretical value of $\Delta\mu_{Ti}$ in the range of -10.3 eV $\leq \Delta\mu_{Ti} \leq 0$ eV. The range for $\Delta\mu_{Nb}$ can be determined more simply. To avoid the competitive formation of secondary dopant oxide Nb_2O_5, $\Delta\mu_{Nb}$ and $\Delta\mu_O$ must satisfy the following condition: $2\Delta\mu_{Nb} + 5\Delta\mu_O < \Delta H_f(Nb_2O_5)$, from which a useful $\Delta\mu_{Nb}$ range can be derived. Together, the ranges for $\Delta\mu_{Ti}$ and $\Delta\mu_{Nb}$ can be used to determine boundary values of $\Delta\gamma$(Nb@Ti) under SrO-rich conditions. We used a similar procedure to calculate $\Delta\gamma$ for substitutional doping of Nb/Ta at interfacial Ti, Al, Sr, or La atoms under two thermodynamic conditions each. Our results for Nb and Ta doping at Sr/La sites are shown in Fig. 1S and 2S of the Supporting Information, respectively, indicate that these substitutions are extremely unfavorable, hence they are not considered further in our work. The results for Nb@Ti and Nb@Al doping are plotted in Fig. 1, while the results for Ta@Ti and Ta@Al doping are plotted in Fig. 2. Several important conclusions can be drawn:

(i) There is very little difference in the energetic favorability of Nb- and Ta-doped interfaces, and either dopant can be stably doped at the LAO/STO interface.

(ii) Of the two viable interfacial doping sites considered, substitutional doping by Nb/Ta is more favorable at the Ti site than that at Al site. In other words, substitution at Ti yields a more stable interface under a wider range of chemical potentials than substitution at Al. However, doping at either site under appropriate thermodynamic conditions can create a more stable interface than in the undoped system.

(iii) Doping at Ti is more favorable under SrO-rich than that under TiO_2-rich conditions, while doping at Al is (slightly) more favorable under La_2O_3-rich than Al_2O_3-rich conditions.

In addition, we also carried out a group of test calculations to evaluate the relative stability of the dopant at a layer different to the interface. Our results show that the Nb@Al and Ta@Al doping at the interface is energetically more favorable than the layer doping far away from the interface, while for the Nb@Ti and Ta@Ti doping, the two layer doping models, *i.e.*, one at the interfacial layer and the other one at the layer far away from the interface have the comparable stability. This indicates the interfacial Nb and Ta layer doping is experimentally feasible.

3.2 Electronic Structure

Here, we investigated the effects of Nb and Ta-doping on the electronic properties of *n*-type LAO/STO HS systems. First, we will provide some insight on the electronic properties of undoped LAO/STO system for comparison, then study the doped systems. It is well-established that 2DEG is primarily derived from the Ti 3*d* orbitals of the first (IF-I) TiO_2 layer of the STO substrate for undoped LAO/STO HS system, along with a small contribution from the third (IF-III) TiO_2 layer near the Fermi level.[18,27,35] The fifth (IF-V) TiO_2 layer has almost no contribution and the other layers away from the interface show an insulating behavior, which shows the typical two-dimensional character of the 2DEG. The width of the metallic region in this abrupt LAO/STO HS system is only ∼9.6 Å along the *c*-axis (∼3 unit cells of the STO). The interfacial (IF-I) TiO_2 layer exhibits a nearly half-metallic nature with a magnetic moment of 0.38 μ_B on the Ti atom. The calculated magnetic moment of the Ti atom in the IF-III TiO_2 layer is 0.08 μ_B and all other layers further away from the interface exhibit no spin-polarization.[18,27,35] For reference, the DOS and layer-resolved DOS of the undoped LAO/STO superlattice system are provided in Fig. 3S the Supporting Information.

To illustrate the effects of Nb and Ta-doping on the electronic properties of the 2DEG in LAO/STO HS, we calculated total and partial DOS projected on Ti 3*d*, Nb 4*d*, and Ta 5*d* orbitals near the interfacial region for Nb@Ti and Ta@Ti doped LAO/STO HS systems in Fig. 3. Total DOS for Nb@Ta (Fig. 3a) and Ta@Ti (Fig. 3b) doped HS systems exhibit typical *n*-type conductivity as found in the case of the abrupt interface and more occupied states near the Fermi energy are found compared to that of the undoped system.[18,27,35] This phenomena can be understood by analyzing the valence states of the dopant. The Nb and Ta atoms typically adopt a +5 valence state, which can be inferred from their respective electron configurations of $4d^45s^1$ and $5d^36s^2$ fillings. When these atoms replace an interfacial Ti^{4+} atom ($3d^24s^2$) in the STO substrate, one free electron will be injected into the system. Our results, however, indicate that Nb and Ta atoms are not in perfect +5

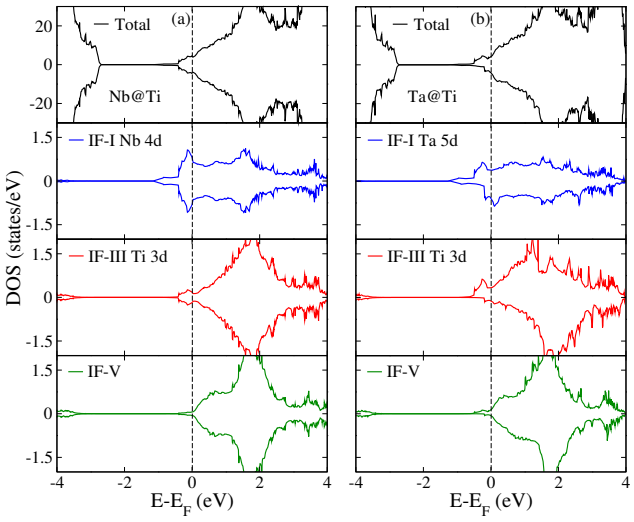

Fig. 3 Calculated spin-polarized total and partial DOS projected on Ti 3*d*, Nb 4*d*, and Ta 5*d* orbitals near the interfacial region of the STO substrate for (a) Nb@Ti and (b) Ta@Ti doped LAO/STO HS systems. The IF-I, IF-III, and IF-V represent the first, third and fifth BO_2 (B = Ti, Nb, and Ta) layers in the STO substrate, respectively. The Fermi level is indicated by the vertical dashed line at 0 eV.

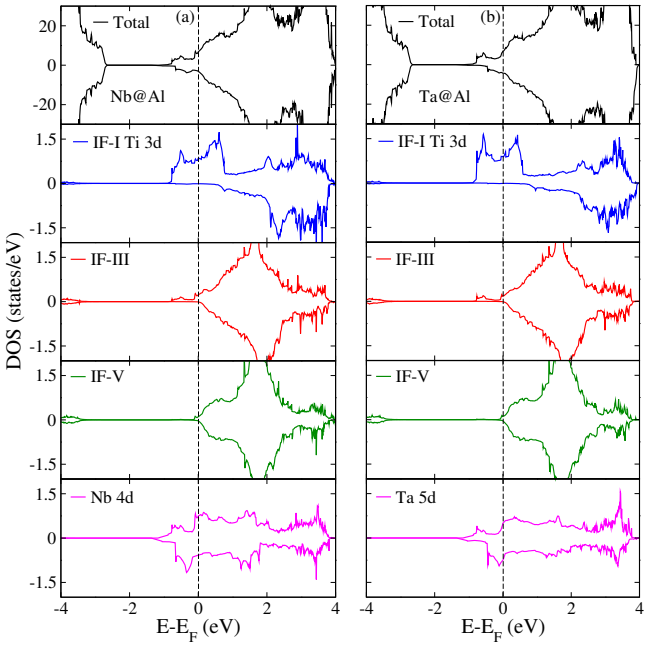

Fig. 4 Calculated spin-polarized total and partial DOS projected on Ti 3*d*, Nb 4*d*, and Ta 5*d* orbitals near the interfacial region of the STO substrate for (a) Nb@Al and (b) Ta@Al doped LAO/STO HS systems.

states after doping since some Nb 4*d* and Ta 5*d* orbitals are occupied, and therefore only a small fraction of free electrons are actually added to the system. Nevertheless, these free electrons still increase the orbital occupation number near Fermi energy, and lead to higher charge carrier density in the doped HS systems compared to the undoped LAO/STO system, as shown below. Moreover, it is found that when Ta is doped at the Ti site (Fig. 3b), the orbital occupation of the total DOS is higher than that of the Nb@Ti (Fig. 3a) doped system, because 5*d* orbital is more de-localized than 4*d* orbital. Therefore, the Ta atom releases more free electrons to the system than the Nb atom. From the partial DOS, one can also see that Nb 4*d* and Ta 5*d* orbitals are also crossing the Fermi level and significantly contributing to the interfacial conductivity. The 2DEG spans only 2 unit cells of the STO substrate, while Ti atoms from the third (IF-III) TiO_2 layers showing a very small orbital occupation. Surprisingly, our results further indicate that when Nb is doped at the Ti site (Fig. 3a), the system shows no spin-polarization, as spin-up and spin-down channels have the identical DOS compared to Ta@Ti (Fig. 3b) doped and undoped LAO/STO HS systems. [18,27,35]

Fig. 4a and 4b represent the total and partial Ti 3*d*, Nb 4*d*, and Ta 5*d* DOS for Nb@Al and Ta@Al doped LAO/STO HS systems, respectively. Our results exhibit that when Nb and Ta atoms substitute for Al, more electrons are added to the system than in the case of Nb@Ti (Fig. 3a) or Ta@Ti (Fig. 3b) doping. This is due to the different valence states of the substituted atoms: Al^{3+} versus Ti^{4+}. That is to say, the Nb@Al (Ta@Al) doping can release one more electron into the LAO/STO HS system than the Nb@Ti (Ta@Ti) doping. Thus substitution at Al substantially enhances the 2DEG orbital occupation near the Fermi energy, charge carrier density, and magnetism of the system. The extra free electrons provided by the Nb and Ta atoms reside almost entirely at the interfacial Ti atoms, see Fig. 4a and 4b. Fig. 4b (Ta@Al) shows that partial occupation of the total and interfacial Ti atoms (IF-I) are higher than that of the Nb@Al doped system (Fig. 4a). This means that the Ta atoms release more free electrons to the system than the Nb dopant, as found in the previous doped systems (discussed in Fig. 3). The Nb 4*d* and Ta 5*d* states cross the Fermi level and contribute to the interfacial conductivity, similar to Nb@Ti and Ta@Ti LAO/STO doped systems. In both doped systems, the partial DOS also indicates that electrons are confined almost within 1.5 unit cells of the STO substrate along the *c*-direction, which is almost half the width of metallic region in the undoped LAO/STO system. [18,27,35] This means that electron transfer from the polar $(LaO)^{+1}$ layer and the Nb/Ta atoms extends only as deep as the nonpolar $(TiO_2)^0$ IF-III layer of the substrate, with transfer to all deeper layers strongly restricted. Therefore, in the doped systems, mobile electrons reside in the first two unit cells of the STO substrate. Finally, one can notice that the shape of

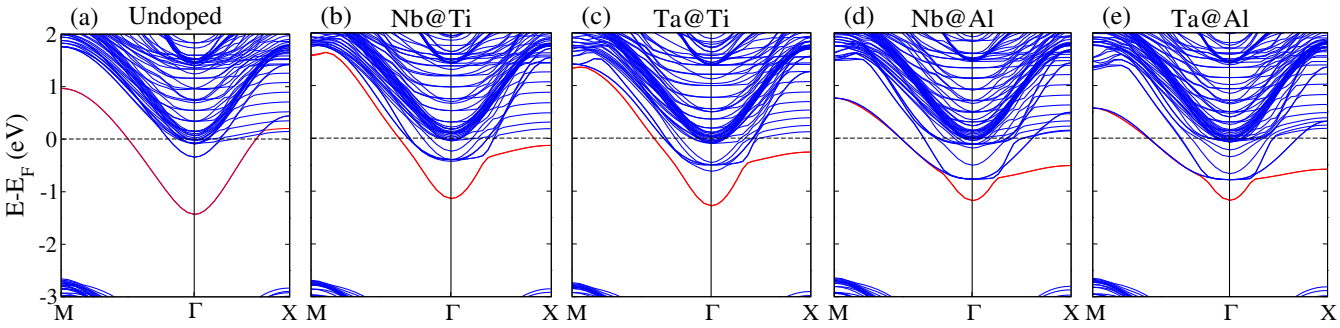

Fig. 5 Calculated band structure for undoped and Nb(Ta)-doped LAO/STO HS systems. The red highlighted lines indicate the specific band used for each of our effective mass calculations.

the DOS in these doped system is very different from that of the undoped LAO/STO HS system.[18,26,27,35] This is because, besides the d_{xy} orbital, d_{yz} orbital of Ti ions also contribute to the formation of the 2DEG, which lead to the different shape of the DOS. More detail behind this phenomenon will be discussed later.

Fig. 5 shows the band structure along the Brillouin Zone path M-Γ-X for all the doped and undoped HS systems. It clearly shows that Nb(Ta)@Ti doping leads to additional occupied bands relative to the undoped system, while Nb(Ta)@Al doping causes more occupied bands. As discussed above, this can be easily understood when considering the valence states of the dopant and host atoms: $Nb(Ta)^{+5}@Ti^{+4}$ doping leads to approximately one free electron per dopant atom, whereas $Nb(Ta)^{+5}@Al^{+3}$ leads to roughly two free electrons per dopant atom. To partially evaluate the Nb(Ta) doping influence on the charge carrier mobility, we then calculated the relative electron effective masses (m_e^*/m_0) using parabolic effective-mass approximation for the minimum conduction bands from M to Γ, i.e, the highlighted bands in the Fig. 5. m_0 refers to the free electron rest mass. For comparison, we also calculated the relative effective mass for the undoped LAO/STO system. The calculated value for the undoped system is 0.59, which is in a good agreement with the previous reported value.[57–59] Note that the calculated effective mass value cannot be directed related to the the absolute electron mobility in the experiment. Rather, it is included as a baseline to which the doped results may be compared, which can provide us a qualitative evaluation whether the Nb and Ta doping can change the electron effective mass and the resulting electron mobility. The calculated relative effective masses for Nb@Ti, Ta@Ti, Nb@Al, and Ta@Al doped systems are 0.36, 0.41, 0.56, and 0.58, respectively. These results indicate that Nb@Ti and Ta@Ti doping can reduce the electron effective mass with respect to that of the undoped system and thus potentially improve the electron mobility, while Nb@Al and Ta@Al doping yield comparable effective mass with that of the undoped system and thus is not beneficial for improving the electron mobility.

3.3 Electron Carrier Density and Interfacial Magnetic Moment

For a qualitative comparison of the various Nb and Ta-doped systems, we determined their total charge carrier density (a) and magnetic moments on Ti atoms near the interfacial region (b) in Fig. 6. To do this, we computed the partial occupation by integrating the conducting states of the total DOS below the Fermi level and then continued to calculate the charge carrier density in each case. The estimated values of occupation numbers and their corresponding charge carrier densities are plotted in Fig. 6a for undoped and Nb(Ta)-doped LAO/STO HS systems. Our calculations show that the highest orbital occupation numbers and charge carrier densities are achieved in Ta@Al doped LAO/STO HS system. As we mentioned above, this happens because when Ta replaces Al, it donates more extra electrons to the system compared to Nb@Al doping, which extensively increases the orbital occupation number of DOS near the Fermi energy (Figure 4b) and hence, raises the charge carrier density. Similarly, the estimated occupation number of Ti atom from interfacial TiO_2 layers in the STO substrate for Nb@Al and Ta@Al doped LAO/STO HS systems are 0.57 and 0.74, respectively, and the corresponding electron carrier densities are 3.7×10^{14} cm^{-2} and 4.9×10^{14} cm^{-2}, larger than that in the undoped superlattice model of about 1.9×10^{14} cm^{-2}.[18] These results also confirm that Ta atoms release more electrons into the system compared to Nb and that these electrons primarily reside at the interfacial Ti atoms, as shown in Fig. 4.

Next, we study the effects of Nb and Ta-doping on the magnetic moments of interfacial Ti atoms in the above mentioned doped HS systems. It is very well known that magnetic moments on interfacial Ti atoms are caused by the partially occupied Ti 3*d* orbitals.[18,27,35,60,61] Therefore, we plotted local magnetic moments on Ti atoms from the IF-I and IF-III TiO_2 layers for undoped and Nb(Ta)-doped LAO/STO HS systems

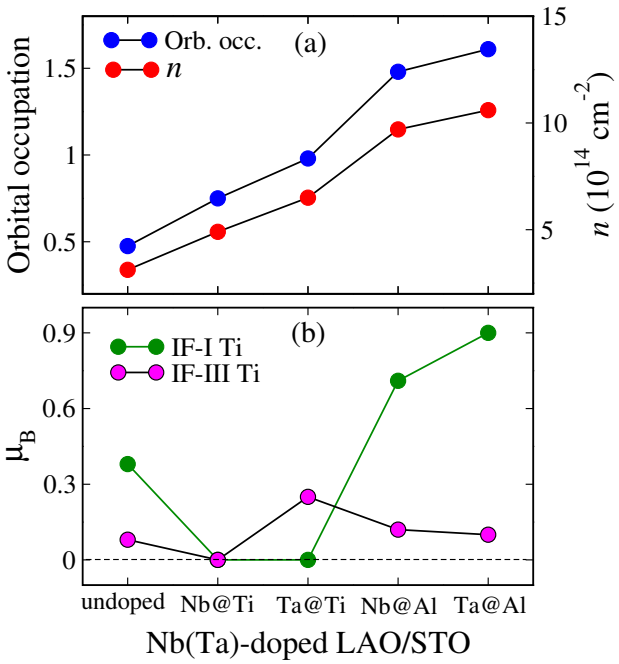

Fig. 6 Calculated (a) total orbital occupation (Orb. occ.) numbers (blue) and corresponding charge carrier densities n (red) and (b) total magnetic moments in undoped and Nb(Ta)-doped LAO/STO HS systems.

in Fig. 6b. The system with Ta-doping at the Al site (Ta@Al) has the largest interfacial (IF-I) Ti magnetic moments compared to undoped and other doped LAO/ST HS systems. For the Nb@Al and Ta@Al doped LAO/STO HS systems, the Ti atoms in IF-III TiO_2 layers show very small spin-polarization with magnetic moments of 0.12 μ_B and 0.10 μ_B, respectively. This is because less electrons transfer to the IF-III layers than that to the IF-I from the LaO layer and also from Nb/Ta doped atoms. The TiO_2 layers further away from the interface in the STO substrate show no spin-polarization. For the Ta@Ti doped system, a significant magnetic moment of 0.25 μ_B is also found in the third (IF-III) TiO_2 layer, while Nb@Ti doped system exhibits no spin-polarization as reflected in the DOS of Fig. 3a.

3.4 Three-Dimensional Charge Density

To gain deep insight into the interfacial metallic states and to visualize the charge transfer effects in the Nb (Ta)-doped LAO/STO systems, we plotted the three-dimensional charge density projected on the bands forming the 2DEG for undoped (a), Nb@Ti (b), Ta@Ti (c), Nb@Al (d), and Ta@Al (e) doped LAO/STO HS systems in Fig. 7. Our results clearly demonstrate that in the undoped LAO/STO HS system, electrons from the polar $(LaO)^{+1}$ layer are mainly transferred to IF-I and IF-III $(TiO_2)^0$ layers of the STO substrate, along with a minor distribution on the IF-V layer (see Fig. 7a), which means that the 2DEG extends within 3 unit cells of the STO substrate along the c-axis, indicating a typical two-dimensional character of conducting states.

In the case of Nb@Ti (Fig. 7b) and Ta@Ti (Fig. 7c) doped systems, 2DEG primarily comes from interfacial Nb and Ta atoms, along with a substantial contribution from the IF-III TiO_2 layers. Interestingly, it is noted that the density of Ti atoms in the second TiO_2 layer (IF-III) is higher in Ta@Ti doped system than in the Nb@Ti system. The third TiO_2 layer (IF-V) in the Nb@Ti doped system has almost no contribution to the interface conductivity, yet in the Ta@Ti doped system it contributes significantly. This difference implies that a few electrons transfer to the deeper STO substrate, consistent with the calculated partial DOS in Fig. 3. One reason is probably because that Ta 5d orbitals are less localized than Nb 4d and thus the Ta 5d orbitals hold less electrons, and the remaining electrons are further transferred to deep TiO_2 layers. As discussed below, another reason is because the structural distortion of the TiO_6 octahedra near the interface in the Ta@Ti system is stronger than that in the Nb@Ti system. For the Nb@Al (Fig. 7d) and Ta@Al (Fig. 7e) doped LAO/STO, the conducting metallic states are mainly contributed by the Nb and Ta atoms, and the interfacial TiO_2 layer (IF-I) in each system.

Table 2 Calculated O-Ti-O bond angles in the ab-plane at IF-III and IF-V TiO_2 layers for undoped, Nb@Ti, Ta@Ti, Nb@Al, and Ta@Al doped LAO/STO HS systems.

	Undoped	Nb@Ti	Ta@Ti	Nb@Al	Ta@Al
IF-III	177.6^o	177.5^o	175.5^o	178.8^o	179.3^o
IF-V	178.7^o	178.8^o	177.9^o	179.3^o	179.5^o

The spatial extension of the 2DEG along the c-direction strongly depends on TiO_6 octahedral distortion in the STO substrate. To elucidate this distortion in our systems, we calculated the O−Ti−O bond angles in the ab-plane at the IF-III and IF-V TiO_2 layers for undoped, Nb@Ti, Ta@Ti, Nb@Al, and Ta@Ti doped LAO/STO HS systems in Table 2. One can clearly see that the TiO_6 octahedra are distorted up to the 3rd TiO_2 layer (IF-V) in the case of the undoped and Nb@Ti doped LAO/STO HS systems. Therefore, charge transfer from the polar $(LaO)^+$ layer to nonpolar $(TiO_2)^0$ layers extends to 3 unit cells of the STO substrate as shown in our charge density plot (Fig. 7a). Similarly, TiO_6 octahedra are distorted up to 3 unit cells of the STO substrate in the Ta@Ti doped system (Fig. 6c), but in the fifth (IF-V) TiO_2 layer the degree of distortion is higher than in the undoped and Nb@Ti doped systems (Fig. 7a and 7b). Therefore, more charge is transferred to the IF-V TiO_2 layer in this case, consistent with the

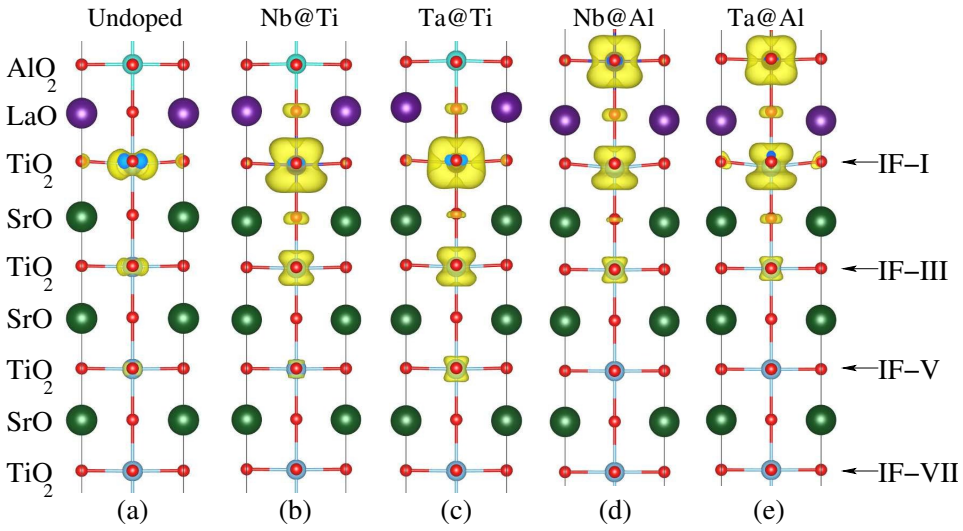

Fig. 7 Charge density projected on the bands forming the metallic states near the interfacial region for undoped (a), Nb@Ti (b), Ta@Ti (c), Nb@Al (d), and Ta@Al (e) doped LAO/STO HS systems.

DOS in Fig. 3. On the other hand, for the Nb@Al and Ta@Al doped HS systems, very small TiO_6 octahedral distortions are found at the IF-III TiO_2 layer, with almost negligible distortions at the IF-V TiO_2 layers. Hence, less charge migrates to deeper TiO_2 layers and a highly confined 2DEG is obtained. Moreover, the density on the Ti atoms in the interfacial TiO_2 layer (IF-I) is larger in the Ta@Al doped system than in the Nb@Al system, which means higher orbital occupation and higher charge carrier density. This is because TiO_6 octahedra is more distorted at the interfacial (IF-I) TiO_2 layer for the Ta@Al doped system than in the undoped and Nb@Al doped LAO/STO HS systems. In short, the Nb and Ta doping at Al sites can significantly modify the electron transport properties of the LAO/STO HS system.

In addition, from the Fig. 6 (charge density), one can see that the occupied Ti 3*d* orbitals in the STO substrate differ in shape compared to the undoped HS system.[18,27,35] This means that the 3*d* bands, which form the 2DEG in doped LAO/STO HS systems, have different orbital occupations. To verify this difference, we plotted the orbital-resolved DOS of Ti 3*d*, Nb 4*d*, and Ta 5*d* states for the Nb@Al (a) and Ta@Al (b) doped LAO/STO HS systems in Fig. 8. As previous results[18,27,35,62,63] indicate, 2DEG resides in the *ab*-plane in the undoped LAO(LTO)/STO HS systems and only the d_{xy} orbitals of interfacial Ti atoms cross the Fermi level, while the d_{yz}/d_{xz} orbitals remain unoccupied. This can be explained in the context of crystal field theory. It is well known that in a regular octahedral crystal field, Ti 3*d* states are split into triply t_{2g} (d_{xy}, d_{xz}, and d_{yz}) and doubly e_g ($d_{3z^2-r^2}$ and $d_{x^2-y^2}$) degenerate states. After structural relaxation, the TiO_6 octahedral distortion results in a degraded symmetry. Therefore,

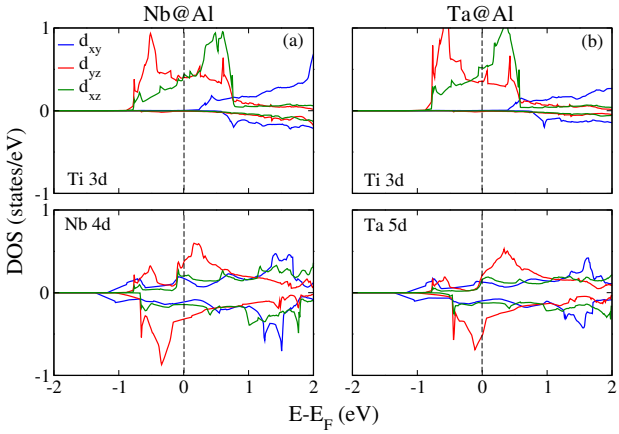

Fig. 8 Orbital-resolved interfacial (IF-I) Ti 3d, Nb 4d, and Ta 5d DOS in Nb@Al (a) and Ta@Al (b) doped LAO/STO HS systems.

the triply degenerate t_{2g} states are split into non-degenerate d_{xy}, d_{yz}, and d_{xz} orbitals, and the transferred electron eventually occupies the low-energy d_{xy} orbitals. For comparison, the orbital-resolved DOS of interfacial (IF-I) Ti atoms for Nb@Al (a) and Ta@Al (b) doped LAO/STO HS systems is shown in Fig. 7. For Nb@Al (Fig. 7a) and Ta@Al (Fig. 7b), one can clearly see that the metallicity results from the admixture of d_{yz} and d_{xz} instead of d_{xy} orbitals, while d_{xy} orbitals remain unoccupied and stay at higher energies in the conduction band (far away from the Fermi level). Therefore, the 2DEG resides in the *yz* and *zx*, rather than *xy*, plane, the reverse of what is usually observed in undoped STO-based HS systems.[18,27,35,62,63] In contrast, both the d_{xy}, d_{xz}, and d_{yz} orbitals

of Nb 4*d* and Ta 5*d* contribute to the interfacial conductivity.

4 CONCLUSION

In summary, first-principles density functional theory calculations were performed to investigate the Nb (Ta) doping effects on the interface energetics and electronic properties of 2DEG in LAO/STO HS system. Our calculations reveal that LAO/STO HS systems with Nb@Ti and Ta@Ti doping is energetically more favorable than the undoped and other doped ones. We found that Nb(Ta)@Ti and Nb(Ta)@Al doping significantly improve the orbital occupation near the Fermi level, and produce a high interfacial charge carrier density. This is mostly attributed to the additional free electrons provided by Nb(Ta) dopant, and these free electrons reside mainly at the Nb(Ta) dopant and the Ti atoms in the interfacial TiO_2 layer of the STO substrate. Our results indicate that the Nb(Ta)@Al doped HS systems exhibit higher interfacial charge carrier density and magnetic moments than the undoped and other doped ones, while the Nb(Ta)@Ti doped HS systems may show higher charge carrier mobility because of the lower electron effective mass. Our theoretical calculations demand an experimental characterization of Nb and Ta-doped LAO/STO systems to fully understand its thermodynamic stability and electron transport property.

5 Acknowledgment

This work is partially supported by a Department of Defense National Security Science and Engineering Faculty Fellowship (under the ONR contract no. N000141510030). KY acknowledges support by start-up funds from the University of California, San Diego.

References

1 A. Ohtomo and H. Y. Hwang, *Nature*, 2004, **427**, 423–426.
2 L. Li, C. Richter, J. Mannhart and R. C. Ashoori, *Nat. Phys.*, 2011, **7**, 762–766.
3 J. A. Bert, B. Kalisky, C. Bell, M. Kim, Y. Hikita, H. Y. Hwang and K. A. Moler, *Nat. Phys.*, 2011, **7**, 767–771.
4 D. A. Dikin, M. Mehta, C. W., C. M. Folkman, C. B. Eom and V. Chandrasekhar, *Phys. Rev. Lett.*, 2011, **107**, 056802.
5 B. Kalisky, J. A. Bert, B. B. Klopfer, C. Bell, H. K. Sato, M. Hosoda, Y. Hikita, H. Y. Hwang and K. A. Moler, *Nat. Commun.*, 2012, **3**, 922.
6 J. S. Lee, Y. W. Xie, H. K. Sato, C. Bell, Y. Hikita, H. Y. Hwang and C. C. Kao, *Nat. Mater.*, 2013, **12**, 703–706.
7 A. Brinkman, M. Huijben, M. van Zalk, J. Huijben, U. Zeitler, J. C. Maan, W. G. van der Wiel, G. Rijnders, D. H. A. Blank and H. Hilgenkamp, *Nat. Mater.*, 2007, **6**, 493–496.
8 G. Herranz, M. Basletić, M. Bibes, C. Carrétéro, E. Tafra, E. Jacquet, K. Bouzehouane, C. Deranlot, A. Hamzi, J.-M. Broto, A. Barthélémy and A. Fert, *Phys. Rev. Lett.*, 2007, **98**, 216803.
9 S. Thiel, G. Hammerl, A. Schmehl, C. W. Schneider and J. Mannhart, *Science*, 2006, **313**, 1942–1945.
10 A. D. Caviglia, S. Gariglio, N. Reyren, D. Jaccard, T. Schneider, M. Gabay, S. Thiel, G. Hammerl, J. Mannhart and J. M. Triscone, *Nature*, 2008, **456**, 624–627.
11 C. Cen, S. Thiel, G. Hammerl, C. W. Schneider, K. E. Andersen, C. S. Hellberg, J. Mannhart and J. Levy, *Nat. Mater.*, 2008, **7**, 298–302.
12 N. Pavlenko, T. Kopp, E. Y. Tsymbal, G. A. Sawatzky and J. Mannhart, *Phys. Rev. B*, 2012, **85**, 020407.
13 M. Salluzzo, S. Gariglio, D. Stornaiuolo, V. Sessi, S. Rusponi, C. Piamonteze, G. M. De Luca, M. Minola, D. Marré, A. Gadaleta, H. Brune, F. Nolting, N. B. Brookes and G. Ghiringhelli, *Phys. Rev. Lett.*, 2013, **111**, 087204.
14 L. Yu and A. Zunger, *Nat. Commun.*, 2014, **5**, 5118.
15 Z. Liu, C. Li, W. Lü, X. Huang, Z. Huang, S. Zeng, X. Qiu, L. Huang, A. Annadi, J. Chen, J. Coey, T. Venkatesan and Ariando, *Phys. Rev. X*, 2013, **3**, 021010.
16 N. Nakagawa, H. Y. Hwang and D. A. Muller, *Nat. Mater.*, 2006, **5**, 204–209.
17 L. Qiao, T. C. Droubay, V. Shutthanandan, Z. Zhu, P. V. Sushko and S. A. Chambers, *J. Phys.: Condens. Matter*, **22**, 312201.
18 S. Nazir, M. Behtash and K. Yang, *Appl. Phys. Lett.*, 2014, **105**, 141602.
19 C. W. Bark, D. A. Felker, Y. Wang, Y. Zhang, H. W. Jang, C. M. Folkman, J. W. Park, S. H. Baek, H. Zhou, D. D. Fong, X. Q. Pan, E. Y. Tsymbal, M. S. Rzchowski and C. B. Eom, *Proc. Natl. Acad. Sci. U.S.A.*, 2011, **108**, 4720–4724.
20 M. Hosoda, C. Bell, Y. Hikita and H. Y. Hwang, *Appl. Phys. Lett.*, 2013, **102**, 091601.
21 B. Kalisky, E. M. Spanton, H. Noad, J. R. Kirtley, K. C. Nowack, C. Bell, H. K. Sato, M. Hosoda, Y. Xie, Y. Hikita, C. Woltmann, G. Pfanzelt, R. Jany, C. Richter, H. Y. Hwang, J. Mannhart and K. A. Moler, *Nat. Mater.*, 2013, **12**, 1091–1095.
22 T. Yajima, Y. Hikita and H. Y. Hwang, *Nat. Mater.*, 2011, **10**, 198–201.
23 N. Reyren, S. Thiel, A. D. Caviglia, L. F. Kourkoutis, G. Hammer, C. Richter, C. W. Schneider, T. Kopp, A. S. Rüetschi, D. Jaccard, M. Gabay, D. A. Muller, J. M.

Triscone and J. Mannhart, *Science*, 2007, **317**, 1196–1199.
24 A. Rastogi, A. K. Kushwaha, T. Shiyani, A. Gangawar and R. C. Budhani, *Adv. Mater.*, 2010, **22**, 4448–4451.
25 A. Rastogi, J. J. Pulikkotil and R. C. Budhani, *Phys. Rev. B*, 2014, **89**, 125127.
26 S. Nazir and K. Yang, *ACS Appl. Mater. Interfaces*, 2014, **6**, 22351–22358.
27 S. Nazir, M. Behtash and K. Yang, *RSC Adv.,*, 2015, **5**, 15682–15689.
28 T. Fix, J. L. MacManus-Driscoll and M. G. Blamire, *Appl. Phys. Lett.*, 2009, **94**, 172101.
29 T. Fix, F. Schoofs, J. L. MacManus-Driscoll and M. G. Blamire, *Appl. Phys. Lett.*, 2010, **97**, 072110.
30 W. S. Choi, S. Lee, V. R. Cooper and H. N. Lee, *Nano Lett.*, 2012, **12**, 4590–4594.
31 F. Schoofs, M. Egilmez, T. Fix, J. L. MacManus-Driscoll and M. G. Blamire, *Solid State Commun.*, 2013, **156**, 35–37.
32 A. S. Disa, D. P. Kumah, A. Malashevich, H. Chen, D. A. Arena, E. D. Specht, S. Ismail-Beigi, F. J. Walker and C. H. Ahn, *Phys. Rev. Lett.*, 2015, **114**, 026801.
33 S. Frank, A. C. Michael, E. V. Mary, E. Mehmet, F. Thomas, E. K. Josee, J. L. McManus-Driscoll and G. B. Mark, *J. Phys.: Condens. Matter*, 2013, **25**, 175005.
34 S. Nazir, J. Cheng, M. Behtash, J. Luo and K. Yang, *ACS Appl. Mater. Interfaces*, 2015, **7**, 14294–14302.
35 S. Nazir, C. Berna and K. Yang, *ACS Appl. Mater. Interfaces*, 2015, **7**, 5305–5311.
36 Y. Z. Chen, F. Trier, T. Wijnands, R. J. Green, N. Gauquelin, R. Egoavil, D. V. Christensen, G. Koster, M. Huijben, N. Bovet, S. Macke, F. He, R. Sutarto, N. H. Andersen, J. A. Sulpizio, M. Honig, G. E. D. K. Prawiroatmodjo, T. S. Jespersen, S. Linderoth, S. Ilani, J. Verbeeck, G. Van Tendeloo, G. Rijnders, G. A. Sawatzky and N. Pryds, *Nat. Mater.*, 2015, **14**, 801–806.
37 J. Cheng, Y. Wang and K. Yang, *In Preparation*, 2015.
38 Y. Kesong, D. Ying, H. Baibiao and P. F. Yuan, *J. Phys. D: Appl. Phys.*, 2014, **47**, 275101.
39 G. Kresse and J. Furthmüller, *Phys. Rev. B*, 1996, **54**, 11169–11186.
40 J. P. Perdew, K. Burke and M. Ernzerhof, *Phys. Rev. Lett.*, 1996, **77**, 3865–3868.
41 V. I. Anisimov, J. Zaanen and O. K. Andersen, *Phys. Rev. B*, 1991, **44**, 943–954.
42 K. Yang, Y. Dai, B. Huang and Y. P. Feng, *Phys. Rev. B*, 2010, **81**, 033202.
43 R. Pentcheva and W. E. Pickett, *Phys. Rev. B*, 2008, **78**, 205106.
44 R. Arras, V. G. Ruiz, W. E. Pickett and R. Pentcheva, *Phys. Rev. B*, 2012, **85**, 125404.
45 Y. S. Lee, S. J. Moon, S. C. Riggs, M. C. Shapiro, I. R. Fisher, B. W. Fulfer, J. Y. Chan, A. F. Kemper and D. N. Basov, *Phys. Rev. B*, 2013, **87**, 195143.
46 B. G. Janesko, T. M. Henderson and G. E. Scuseria, *J. Phys.: Condens. Matter*, 2009, **11**, 443–454.
47 F. El-Mellouhi, E. N. Brothers, M. J. Lucero and G. E. Scuseria, *Phys. Rev. B*, 2011, **84**, 115122.
48 F. El-Mellouhi, E. N. Brothers, M. J. Lucero, I. W. Bulik and G. E. Scuseria, *Phys. Rev. B*, 2013, **87**, 035107.
49 C. Franchini, *J. Phys.: Condens. Matter*, 2014, **26**, 253202.
50 F. Cossu, U. Schwingenschlögl and V. Eyert, *Phys. Rev. B*, 2013, **88**, 045119.
51 H. W. Jang, D. A. Felker, C. W. Bark, Y. Wang, M. K. Niranjan, C. T. Nelson, Y. Zhang, D. Su, C. M. Folkman, S. H. Baek, S. Lee, K. Janicka, Y. Zhu, X. Q. Pan, D. D. Fong, E. Y. Tsymbal, M. S. Rzchowski and C. B. Eom, *Science*, 2011, **331**, 886–889.
52 D. R. Hamann, D. A. Muller and H. Y. Hwang, *Phys. Rev. B*, 2006, **73**, 195403.
53 S. Okamoto, A. J. Millis and N. A. Spaldin, *Phys. Rev. Lett.*, 2006, **97**, 056802.
54 R. Pentcheva and W. E. Pickett, *Phys. Rev. Lett.*, 2009, **102**, 107602.
55 S. V. Dudiy and B. I. Lundqvist, *Phys. Rev. B*, 2001, **64**, 045403.
56 S. Nazir, J. Cheng, M. Behtash, J. Luo and K. Yang, *ACS Appl. Mater. Interfaces*, 2015, **7**, 14294–14302.
57 N. C. Bristowe, E. Artacho and P. B. Littlewood, *Phys. Rev. B*, 2009, **80**, 045425.
58 P. Delugas, A. Filippetti, V. Fiorentini, D. I. Bilc, D. Fontaine and P. Ghosez, *Phys. Rev. Lett.*, 2011, **106**, 166807.
59 C. Cancellieri, M. L. Reinle-Schmitt, M. Kobayashi, V. N. Strocov, P. R. Willmott, D. Fontaine, P. Ghosez, A. Filippetti, P. Delugas and V. Fiorentini, *Phys. Rev. B*, 2014, **89**, 121412.
60 S. Nazir, M. Behtash and K. Yang, *J. Appl. Phys.*, 2015, **117**, 115305.
61 K. Janicka, J. P. Velev and E. Y. Tsymbal, *J. Appl. Phys.*, 2008, **103**, 07B508.
62 M. Salluzzo, J. C. Cezar, N. B. Brookes, V. Bisogni, G. M. De Luca, C. Richter, S. Thiel, J. Mannhart, M. Huijben, A. Brinkman, G. Rijnders and G. Ghiringhelli, *Phys. Rev. Lett.*, 2009, **102**, 166804.
63 J. H. You and J. H. Lee, *Phys. Rev. B*, 2013, **88**, 155111.

Table of Contents (TOC) Image

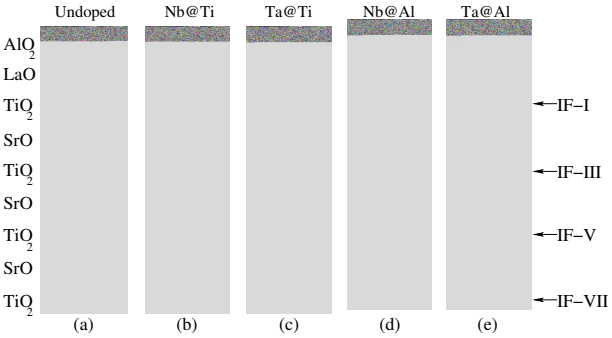

Nb (Ta) layer doping at the interfacial region in the $LaAlO_3/SrTiO_3$ heterostructure system provides a possible avenue to tune the electron transport property of the two-dimensional electron gas.